

# Epigenetic targeting of Hedgehog pathway transcriptional output through BET bromodomain inhibition

Yujie Tang<sup>1,2</sup>, Sharareh Gholamin<sup>2</sup>, Simone Schubert<sup>1,2</sup>, Minde I Willardson<sup>3</sup>, Alex Lee<sup>4</sup>, Pratiti Bandopadhyay<sup>5-8</sup>, Guillaume Bergthold<sup>5-7</sup>, Sabran Masoud<sup>1</sup>, Brian Nguyen<sup>1</sup>, Nujsaubnusi Vue<sup>1</sup>, Brianna Balansay<sup>1</sup>, Furong Yu<sup>1,2</sup>, Sekyung Oh<sup>1,2</sup>, Pamelyn Woo<sup>1</sup>, Spenser Chen<sup>1</sup>, Anitha Ponnuswami<sup>1</sup>, Michelle Monje<sup>1</sup>, Scott X Atwood<sup>4</sup>, Ramon J Whitson<sup>4</sup>, Siddhartha Mitra<sup>2</sup>, Samuel H Cheshier<sup>2</sup>, Jun Qi<sup>9</sup>, Rameen Beroukhim<sup>5,8,9</sup>, Jean Y Tang<sup>4</sup>, Rob Wechsler-Reya<sup>10</sup>, Anthony E Oro<sup>4</sup>, Brian A Link<sup>3</sup>, James E Bradner<sup>5,8,9</sup> & Yoon-Jae Cho<sup>1,2,11</sup>

Hedgehog signaling drives oncogenesis in several cancers, and strategies targeting this pathway have been developed, most notably through inhibition of Smoothed (SMO). However, resistance to Smoothed inhibitors occurs by genetic changes of Smoothed or other downstream Hedgehog components. Here we overcome these resistance mechanisms by modulating *GLI* transcription through inhibition of bromo and extra C-terminal (BET) bromodomain proteins. We show that BRD4 and other BET bromodomain proteins regulate *GLI* transcription downstream of SMO and suppressor of fused (SUFU), and chromatin immunoprecipitation studies reveal that BRD4 directly occupies *GLI1* and *GLI2* promoters, with a substantial decrease in engagement of these sites after treatment with JQ1, a small-molecule inhibitor targeting BRD4. Globally, genes associated with medulloblastoma-specific *GLI1* binding sites are downregulated in response to JQ1 treatment, supporting direct regulation of *GLI* activity by BRD4. Notably, patient- and GEMM (genetically engineered mouse model)-derived Hedgehog-driven tumors (basal cell carcinoma, medulloblastoma and atypical teratoid rhabdoid tumor) respond to JQ1 even when harboring genetic lesions rendering them resistant to Smoothed antagonists. Altogether, our results reveal BET proteins as critical regulators of Hedgehog pathway transcriptional output and nominate BET bromodomain inhibitors as a strategy for treating Hedgehog-driven tumors with emerged or *a priori* resistance to Smoothed antagonists.

The Hedgehog (Hh) pathway is an evolutionarily conserved signaling axis that directs embryonic patterning through strict temporal and spatial regulation of cell proliferation and differentiation<sup>1</sup>. Developmental aberrations in Hh signaling result in dysmorphology, such as cyclopism, holoprosencephaly and limb deformity, when its output is absent or decreased<sup>2</sup> and in cancer predisposition, as is seen in nevoid basal cell carcinoma syndrome (Gorlin syndrome)<sup>3</sup>, when its output is increased or unchecked<sup>1,4</sup>.

In canonical Hh signaling, several morphogens (sonic hedgehog (SHH), Indian hedgehog (IHH) and desert hedgehog (DHH))<sup>5,6</sup> have been identified that bind to the multipass cell-surface receptor Patched (PTCH1)<sup>1</sup>. When not bound by Hh ligand, PTCH1 inhibits the G protein-coupled receptor, SMO<sup>7</sup>. Once bound by ligand, however, PTCH1 no longer inhibits SMO, allowing SMO to positively regulate mobilization of the otherwise latent zinc finger transcription factor *GLI2*, residing in the cilia, to the nucleus, where *GLI2* transactivates the *GLI1* promoter<sup>8-10</sup>. *GLI1* and *GLI2* directly transactivate

transcription of Hh target genes, several of which are involved in proliferation, such as *MYCN* and *CCND1* (ref. 11). *GLI1* also serves to amplify the output of Hh signaling in a positive feedback loop by activating transcription of *GLI2*, albeit indirectly<sup>12</sup>. Ultimately, the transcriptional programs mediated by Hh signaling orchestrate an array of events based on cellular, temporal and spatial context, with perhaps the most phenotypically consequential event being an increase in cell proliferation.

Inappropriate activation of Hh signaling results in tumor formation in several tissue lineages, including skin, brain, muscle, breast and pancreas<sup>13-15</sup>. The tumors most commonly associated with aberrant Hh signaling are basal cell carcinoma (BCC) and medulloblastoma, given their prevalence in individuals with germline mutations in *PTCH1* (Gorlin syndrome)<sup>3,4</sup>. However, the overwhelming majority of Hh-driven BCCs and medulloblastomas activate Hh signaling through sporadic somatic mutations in *PTCH1* or other components of the Hh pathway<sup>14,16,17</sup>. These include activating mutations in *SMO*

<sup>1</sup>Department of Neurology and Neurological Sciences, Stanford University School of Medicine, Stanford, California, USA. <sup>2</sup>Department of Neurosurgery, Stanford University School of Medicine, Stanford, California, USA. <sup>3</sup>Department of Cell Biology, Neurobiology and Anatomy, Medical College of Wisconsin, Milwaukee, Wisconsin, USA. <sup>4</sup>Program in Epithelial Biology, Stanford University School of Medicine, Stanford, California, USA. <sup>5</sup>Department of Cancer Biology, Dana-Farber Cancer Institute, Boston, Massachusetts, USA. <sup>6</sup>Pediatric Neuro-oncology, Department of Pediatric Oncology, Dana-Farber Cancer Institute, Boston, Massachusetts, USA. <sup>7</sup>Division of Pediatric Hematology/Oncology, Boston Children's Hospital, Boston, Massachusetts, USA. <sup>8</sup>Broad Institute of MIT and Harvard, Cambridge, Massachusetts, USA. <sup>9</sup>Department of Medical Oncology, Dana-Farber Cancer Institute, Boston, Massachusetts, USA. <sup>10</sup>Sanford-Burnham Medical Research, La Jolla, California, USA. <sup>11</sup>Stanford Cancer Institute, Stanford University Medical Center, Stanford, California, USA. Correspondence should be addressed to Y.-J.C. (yjcho1@stanford.edu).

Received 18 March; accepted 29 May; published online 29 June 2014; doi:10.1038/nm.3613

or inactivating mutations in *SUFU*, which negatively regulates Hh output downstream of SMO<sup>17,18</sup>. Genomic amplification of *GLI2*, and more rarely *GLI1*, has also been reported and is associated with a more aggressive clinical course<sup>16,19–21</sup>. In addition, noncanonical activation of the Hh pathway can occur through loss of SMARCB1, a component of the SWI/SNF chromatin remodeling complex, which results in derepression of transcriptional activity at the *GLI1* locus in malignant rhabdoid tumors<sup>22</sup>. Similarly, the EWS-FLI fusion oncogene responsible for Ewing sarcoma has been shown to directly transactivate the *GLI1* promoter<sup>23</sup>.

The identification of SMO as the main pharmacological target of cyclopamine<sup>24</sup>, a natural compound found in wild corn lily (*Veratrum californicum*)<sup>2</sup>, fostered the development of clinically optimized compounds with potent activity against SMO<sup>25–27</sup>. Some of these compounds have shown clinical efficacy against BCC, medulloblastoma and other cancers<sup>28–30</sup>. However, emergence of resistance and *a priori* resistance have been encountered<sup>25,29,31</sup>, prompting investigations into alternate strategies targeting new sites on SMO and Hh pathway components downstream of SMO<sup>32,33</sup> or signaling pathways that cooperate with Hh activation in development and disease<sup>25,34,35</sup>. High-throughput screens have also identified scaffolds that regulate GLI processing and its translocation to or from the cilia and nucleus<sup>36</sup>. However, the effectiveness of these strategies against Hh-driven cancers with *MYCN* amplification, such as SHH-subtype medulloblastomas, is unclear, as *MYCN* appears to be epistatic to the targets of many of these drugs.

A new class of drugs targeting BET bromodomain proteins (BRD2–BRD4 and BRDT) was described recently<sup>37</sup>. Bromodomains recognize and bind to  $\epsilon$ -*N*-lysine acetylation motifs on open chromatin, such as those found on K27 residues of H3 histone N-terminal tails<sup>38,39</sup>. The BET proteins also interact with the positive transcription elongation factor (P-TEFb)<sup>40,41</sup> and phosphorylate Ser2 of RNA polymerase II (PolII), facilitating gene transcription at ‘super-enhancer’ sites across the genome<sup>42,43</sup>. BRD-containing complexes that bind at these super-enhancer sites often localize to promoter regions of key transcription factors such as *MYC*, and disruption of these complexes by BET inhibitors has produced substantial responses in mice bearing xenografts of treatment-refractory cancers driven by *MYC* and other previously ‘untargetable’ oncogenes, with limited or no toxicity to normal tissues<sup>44–47</sup>.

Here we aimed to identify whether inhibition of BET bromodomain proteins could provide a strategy for treating Hh-driven tumors, including those resistant to SMO antagonists. We provide evidence that BRD4 is a critical regulator of *GLI1* and *GLI2* transcription through direct occupancy of their promoters. Furthermore, we show that occupancy of *GLI1* and *GLI2* promoters by BRD4 and transcriptional activation at cancer-specific GLI promoter-binding sites are markedly inhibited by the BET inhibitor JQ1. In GEMM- and patient-derived tumors with constitutive Hh pathway activation, JQ1 effectively decreases tumor cell proliferation and viability *in vitro* and *in vivo*, even when genetic lesions conferring resistance to SMO inhibition (SMOi) are present. Notably, the inhibition of cell proliferation by JQ1 can be rescued by *GLI2* expression driven by a plasmid-based cytomegalovirus (CMV) promoter, which, in contrast to endogenous *GLI* promoters, is not under direct transcriptional regulation by BET proteins. In sum, our study identifies BET proteins as epigenetic regulators of Hedgehog transcriptional output and establishes a rationale for the use of BET inhibitors in cancers with evidence of Hh pathway activation.

## RESULTS

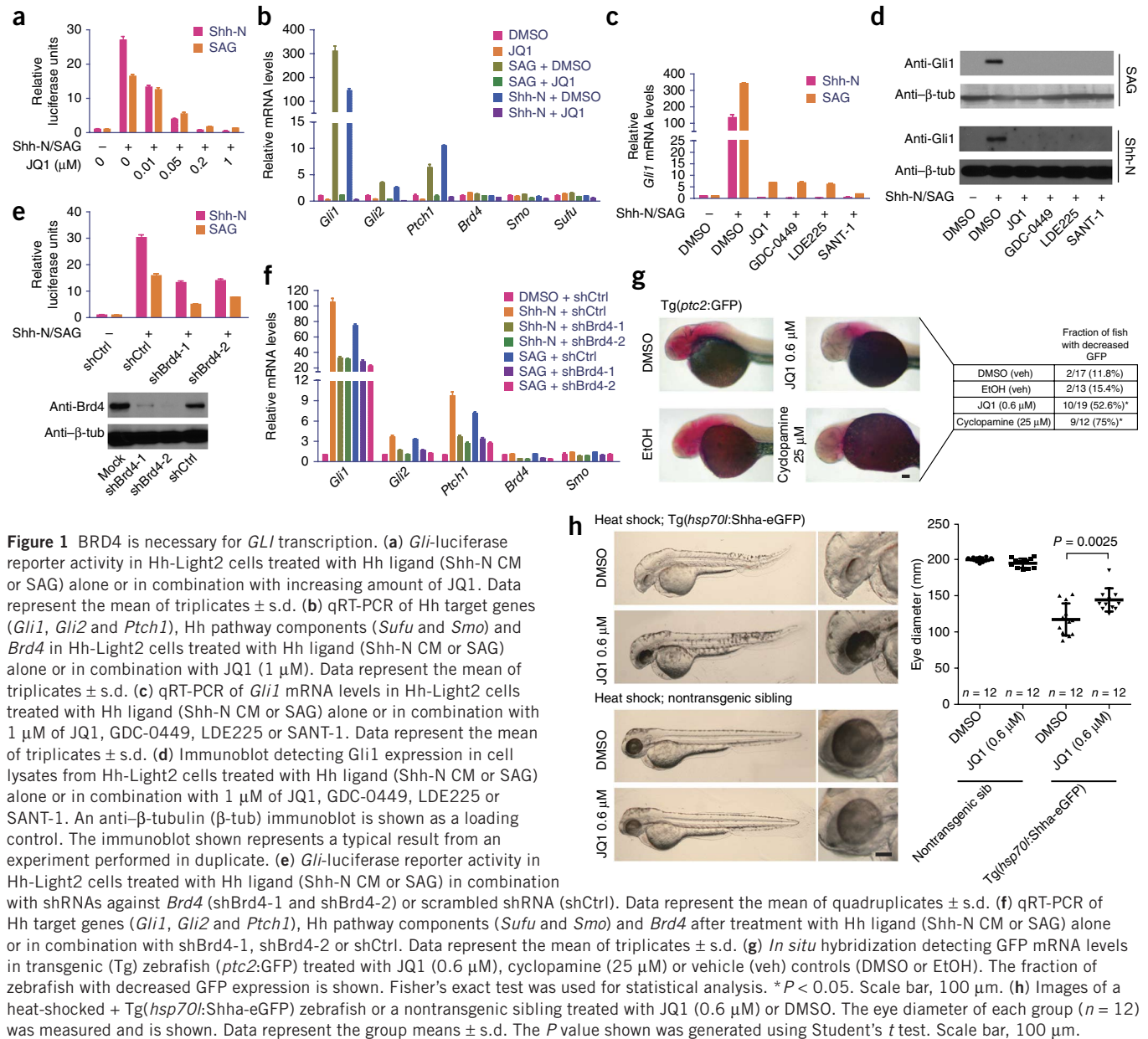
### BRD4 is required for ligand-induced Hh transcriptional output

The BET protein BRD4 enhances the transcription of key genes involved in embryonic stem cell maintenance<sup>42</sup> and oncogenesis<sup>43</sup>. Therefore, we hypothesized that BRD4 is a transcriptional cofactor for Hh-responsive genes. In the mouse 3T3 cell-based Hh-Light2 reporter line containing a stably integrated *Gli*-luciferase reporter construct<sup>48</sup>, ligand-induced activation of Hh-Light2 cells with either Shh-N conditioned medium (CM)<sup>49</sup> or Smoothed agonist (SAG)<sup>48</sup> resulted in an expected increase in *Gli1*-luciferase activity and *Gli1* mRNA levels, which were both potently inhibited by increasing doses of the BET inhibitor JQ1 (Fig. 1a and Supplementary Fig. 1). Upregulation of other Hh target genes such as *Ptch1* and *Gli2* was also inhibited by JQ1 (Fig. 1b). In contrast, *Smo* expression was modestly influenced, and expression of *Sufu* and *Brd4* was not substantially altered by JQ1 (Fig. 1b). Notably, the inhibition of *Gli1* expression by JQ1 equaled that by SMO inhibitors (GDC-0449, LDE225 or SANT-1) (Fig. 1c,d). Additionally, shRNA-mediated knockdown of *Brd4* in Hh-Light2 cells followed by Shh-N CM or SAG stimulation resulted in marked inhibition of ligand-induced *Gli*-luciferase activity and Hh target gene expression, directly supporting an essential role of *Brd4* in Hh signaling (Fig. 1e,f).

To further assess inhibition of Hh transcriptional output by JQ1, we used zebrafish harboring a *ptc2*:GFP reporter transgene, a well-described canonical Hh pathway reporter in zebrafish<sup>50,51</sup>. Embryos exposed to JQ1 from 2 to 30 hours post fertilization (hpf) showed decreased expression of GFP mRNAs, similar to the results seen in cyclopamine-exposed fish (Fig. 1g). We also assessed whether JQ1 could revert abnormal phenotypes caused by aberrant Hh signaling in a temperature-sensitive transgenic fish line harboring an *hsp70l*:Shha-enhanced GFP (eGFP) transgene<sup>51</sup>, which overexpresses Shh and produces a reliable and well-described dysgenic eye phenotype that often includes a ventral coloboma, a structural defect in the eye resulting from improper closure of gaps located between various eye structures during embryonic development<sup>52,53</sup>. As predicted, heat-shocked transgenic fish treated with vehicle alone (DMSO) developed abnormally shaped eyes with diminished diameter relative to their heat-shocked nontransgenic siblings (Fig. 1h). However, fish exposed to JQ1 immediately after heat shock trended toward more normal-appearing eyes with statistically significant increases in eye diameter, suggesting that BET inhibition countered the effects of aberrant Hh signaling *in vivo* in this model (Fig. 1h).

### BRD4 regulates Hh signaling at *Gli1* and *Gli2* promoters

We next examined the effects of JQ1 on Hh signaling in *Sufu*<sup>-/-</sup> mouse embryonic fibroblasts (MEFs)<sup>54</sup> and Hh-Light2 cells overexpressing *GLI2*. *SUFU* positively regulates the degradation of GLI proteins<sup>54</sup>, and thus loss of *SUFU* activity results in stabilization of GLI and constitutive Hh signaling downstream of SMO. As expected, we observed markedly increased *Gli1* mRNA and protein levels in *Sufu*<sup>-/-</sup> MEFs, which were substantially downregulated by JQ1 (Fig. 2a,c and Supplementary Fig. 2a,b). We also noted decreased transcription of *Gli2*, as well as *Smo* to a lesser extent, after JQ1 treatment, whereas *Brd4* mRNA levels remained unchanged (Fig. 2a). In stark contrast to JQ1 treatment, we observed little to no effect on *Gli* transcripts or *Gli1* protein levels in *Sufu*<sup>-/-</sup> MEFs after treatment with the SMO inhibitors (LDE225, GDC-0449 or SANT-1) (Fig. 2b,c). Consistent with pharmacological inhibition of *Brd4*, shRNA-mediated knockdown of *Brd4* in *Sufu*<sup>-/-</sup> MEFs resulted in



decreased *Gli1* and *Gli2* mRNA levels (Fig. 2d). It is worth noting that *Brd4* knockdown did not abrogate GLI-luciferase activity or *Gli* expression as effectively as did JQ1 treatment. This result could be explained by incomplete knockdown of *Brd4*, or it could suggest that other BET proteins (all targets of JQ1) may also contribute to the transcriptional regulation of *Gli* genes. Indeed, knockdown of either *Brd2* or *Brd3* resulted in a substantial decrease of *Gli* mRNA levels in *Sufu*<sup>-/-</sup> MEFs (Supplementary Fig. 2c).

In Hh-Light2 cells, forced expression of full-length mouse *Gli2* (hemagglutinin (HA)-*Gli2*-FL) or an N-terminally truncated active form of human *GLI2* (Myc-*GLI2*-DN)<sup>55</sup> resulted in an increase in *Gli1* mRNA levels, which was inhibited by JQ1 but not SMO inhibitors (GDC-0449, LDE225 or SANT-1) (Fig. 2e). Notably, we did not observe any decrease in ectopic *GLI2* expression driven by the CMV promoter expression construct after JQ1 treatment, in contrast to the marked decrease in endogenous *Gli* transcripts (Figs. 1b and 2f). Additionally, upregulation of *Ptch1*, another Hh target gene, was not inhibited by

JQ1, suggesting that not all Hh target genes are directly dependent on *Brd4*, as *Gli* genes themselves are (Supplementary Fig. 2d).

In *Sufu*<sup>-/-</sup> cells, JQ1 decreased *Gli1* and *Gli2* levels as early as 3 h after treatment, supporting a role for *Brd4* as a transcriptional cofactor that directly regulates transactivation of *Gli* promoters (Supplementary Fig. 2e). Chromatin immunoprecipitation followed by quantitative PCR (ChIP-qPCR) using antibody to *Brd4* of regions flanking the transcription start sites of *Gli1* and *Gli2* promoters confirmed increased *Brd4* occupancy at both *Gli* promoters after SAG-mediated activation of Hh signaling in Hh-Light2 cells (Fig. 2g,h). Accordingly, ChIP-qPCR with antibody to PolII showed engagement of both *Gli* promoters by PolII after SAG stimulation. Notably, both *Brd4* and PolII interactions at the *Gli* promoters were blocked by the addition of JQ1 (Fig. 2g,h). Similarly, in *Sufu*<sup>-/-</sup> MEFs, we observed increased baseline occupancy of *Gli* promoters by *Brd4* and PolII relative to that in wild-type (WT) MEFs, which was markedly inhibited by JQ1 (Fig. 2i,j).

### JQ1 inhibits *Ptch*-deficient medulloblastoma and BCC

We investigated the efficacy of JQ1 in Hh-driven tumors using cell lines derived from autochthonous medulloblastomas (SmoWT-MB and Med1-MB) arising in *Ptch*<sup>+/-</sup>; *Trp53*<sup>-/-</sup> and *Ptch*<sup>+/-</sup>; *lacZ* mice, respectively<sup>32,56</sup>, and BCC (ASZ001)<sup>57</sup>, also derived from *Ptch*<sup>+/-</sup>

mice. JQ1 treatment resulted in marked downregulation of *Gli* mRNA and protein expression with little to no effect on *Smo*, *Sufu* or *Brd4* (Fig. 3a–d and Supplementary Fig. 3a). Again, we observed a rapid decrease of *Gli* gene expression after JQ1 treatment (as early as 3 h), supporting a direct effect of BET inhibition on *Gli* promoters

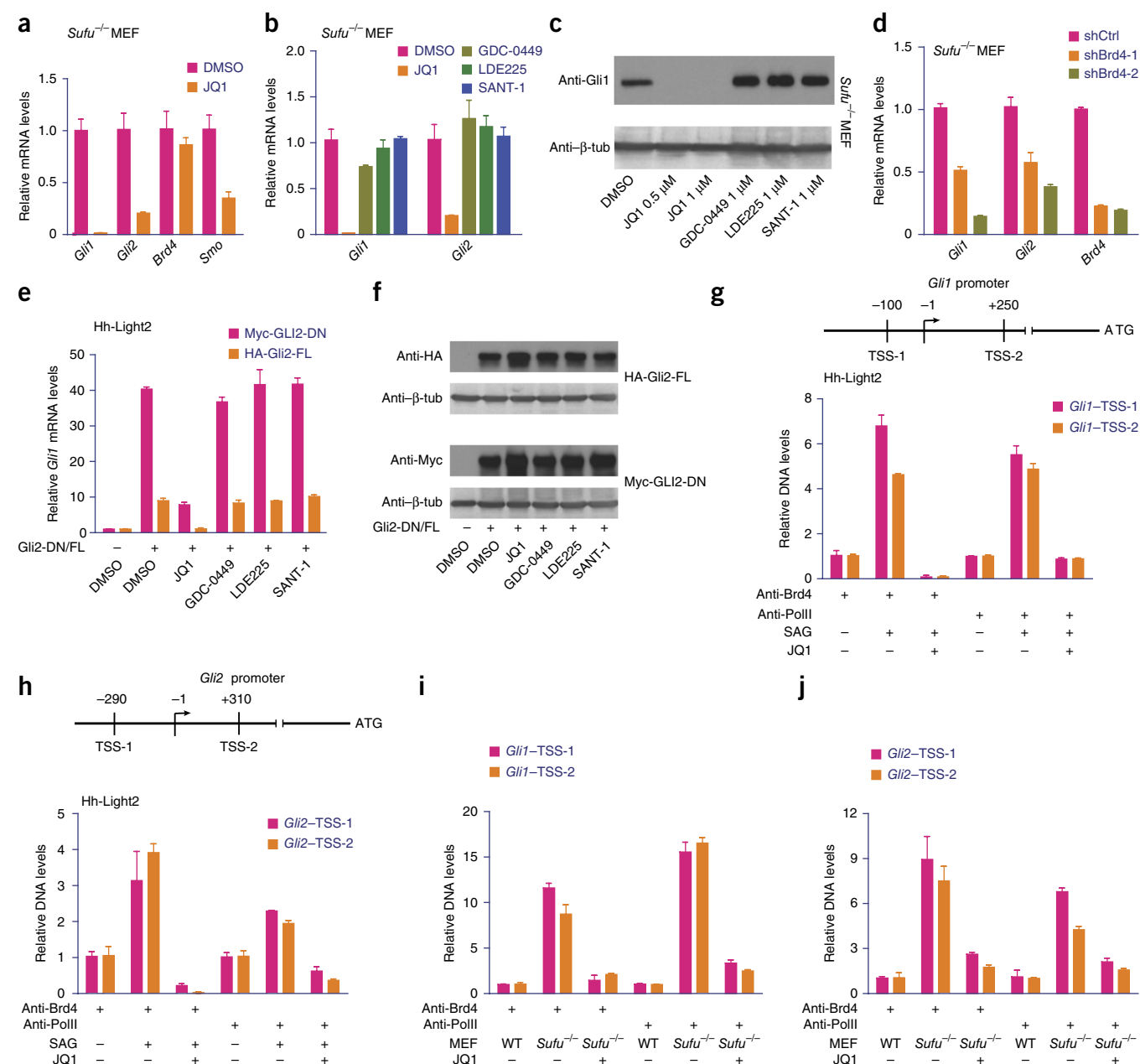


**Figure 2** JQ1 inhibits Hh target gene activation at the level of the *GLI1* and *GLI2* promoters. (a) qRT-PCR showing *Gli1*, *Gli2*, *Smo* and *Brd4* mRNA levels in *Sufu*<sup>-/-</sup> MEFs treated with JQ1. Data represent the mean of triplicates  $\pm$  s.d. (b) *Gli1* and *Gli2* mRNA levels in *Sufu*<sup>-/-</sup> MEFs treated with DMSO, JQ1, GDC-0449, LDE225 or SANT-1. Data represent the mean of triplicates  $\pm$  s.d. (c) Immunoblot detecting GLI1 expression in cell lysates from *Sufu*<sup>-/-</sup> MEFs treated with DMSO, JQ1, GDC-0449, LDE225 or SANT-1. An anti-β-tubulin immunoblot is shown as a loading control. The immunoblots in c and f represent a typical result from each experiment performed in duplicate. (d) qRT-PCR showing *Gli1*, *Gli2* and *Brd4* mRNA levels in *Sufu*<sup>-/-</sup> cells expressing shBrd4-1, shBrd4-2 or shCtrl. Data represent the mean of triplicates  $\pm$  s.d. (e) qRT-PCR showing *Gli1* mRNA levels in Hh-Light2 cells transiently transfected with HA-Gli2-FL or Myc-Gli2-DN and their responses to JQ1, GDC-0449, LDE225 or SANT-1. Data represent the mean of triplicates  $\pm$  s.d. (f) Anti-HA and anti-Myc immunoblots on cell lysates from Hh-Light2 cells transfected with HA-Gli2-FL or Myc-Gli2-DN and treated with DMSO, JQ1, GDC-0449, LDE225 or SANT-1. An anti-β-tubulin immunoblot is shown as a loading control. (g–j) Schematic of regions flanking the *Gli1* and *Gli2* promoter transcription start sites (TSS) analyzed by ChIP-qPCR of Brd4 and PolII occupancies in Hh-Light2 cells treated with SAG and JQ1 (g,h) and in *Sufu*<sup>-/-</sup> MEFs treated with JQ1 (i,j). Data represent the mean of triplicates  $\pm$  s.d. Except where indicated, cells were treated with 1 μM of JQ1, GDC-0449, LDE225 or SANT-1.

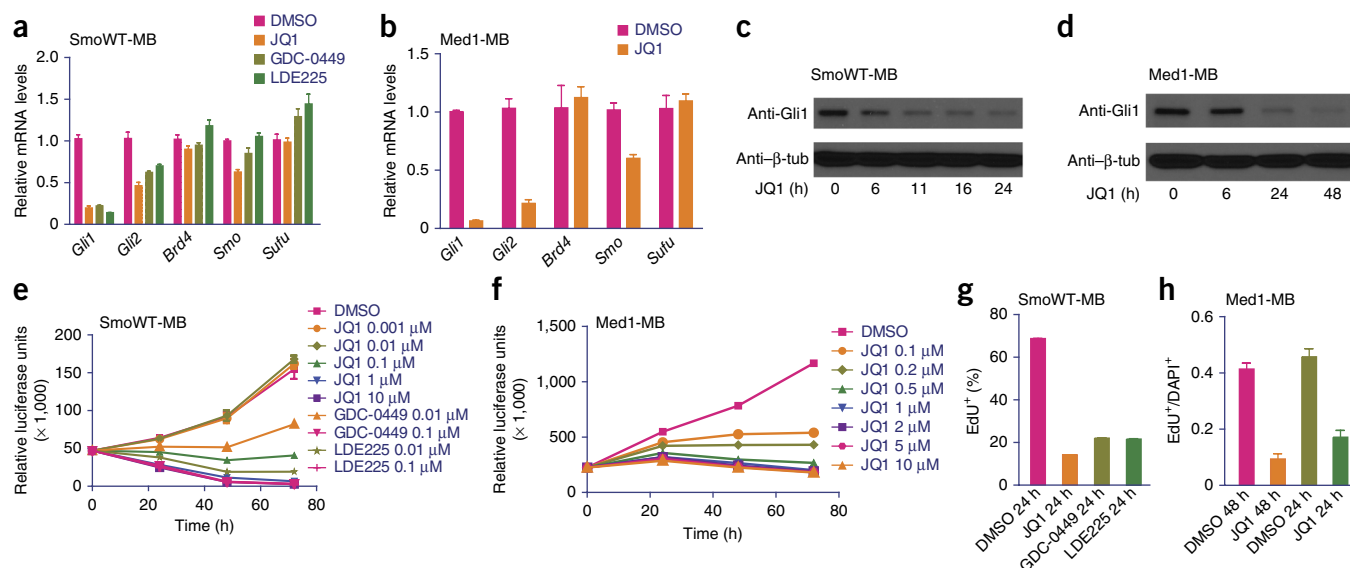


**Figure 3** JQ1 inhibits Hh pathway activity and cell viability and proliferation in Ptch-mutated medulloblastoma (SmoWT-MB and Med1-MB) cells. (a,b) qRT-PCR of the expression of Hh pathway target genes (*Gli1* and *Gli2*), components (*Smo* and *Sufu*) and *Brd4* in SmoWT-MB and Med1-MB cells treated with JQ1 (1 μM), GDC-0449 (0.1 μM) or LDE225 (0.1 μM). Data represent the mean of triplicates ± s.d. (c,d) Immunoblots detecting Gli1 expression in response to JQ1 treatment over time. An anti-β-tubulin immunoblot is shown as a loading control. The immunoblots represent a typical result from each experiment performed in duplicate. (e,f) Cell viability detection over time with increasing doses of JQ1 or SMO inhibitors. Data represent the group means ± s.d. (g,h) Proliferative index in response to JQ1 (1 μM) or SMO inhibitors (GDC-0449 or LDE225 at 0.1 μM) as measured by EdU incorporation. Data represent the group means ± s.d.

(Supplementary Fig. 3b). Accordingly, ChIP-qPCR using antibodies to Brd4 and PolII showed potent inhibition of Brd4 and PolII occupancy at *Gli* promoters in all cell lines after exposure to JQ1 (Supplementary Fig. 3c,d).

In Med1-MB and SmoWT-MB cells, JQ1 treatment resulted in dose-responsive decreases in cell viability to a much greater extent than those observed in Hh-Light2 or *Sufu*<sup>-/-</sup> MEFs (Supplementary Fig. 4a). Potent growth inhibition was achieved (half-maximum inhibitory concentration (IC<sub>50</sub>) ~50–150 nM; Supplementary Fig. 4b,c) with marked decreases of proliferation (Fig. 3e–h), induction of apoptosis (Supplementary Fig. 4d,e) and, in Med1-MB cells, an increased fraction of cells in G1 and a decreased fraction of cells transitioning through S phase (Supplementary Fig. 4f). Notably, in SmoWT-MB cells, the inhibitory effects of JQ1 on *Gli* expression, cell viability and proliferation were equivalent to those of SMO inhibitors (GDC-0449 or LDE225) (Fig. 3a,e,g and Supplementary Figs. 3a and 4d), and these effects were enhanced when we exposed cells to both JQ1 and GDC-0449 in combination (Supplementary Fig. 4g).

Using microarray analysis, we assessed changes in global gene expression in JQ1-treated SmoWT-MB cells compared with DMSO- and GDC0449-treated cells. We observed a substantial overlap between significantly differentially expressed genes ( $P < 0.0001$ ) or gene sets ( $P < 0.0001$ ; Supplementary Dataset) by JQ1 and GDC0449 in both cell lines compared with DMSO-treated controls, including the anticipated GLI target genes *Gli2*, *Ptch1*, *Ccnd1*, *Ccnd2*, *Hhip* and *Cdk6* (Supplementary Fig. 5a–c). We next compared JQ1-induced gene expression profiles with gene sets derived from previously published ChIP-chip studies, which indexed gene promoters with Gli1-binding sites in normal granule neuron precursor cells (GNPs) and *Ptch*<sup>+/-</sup> medulloblastoma cells<sup>58</sup>. Specifically, we analyzed for enrichment of ChIP-chip peaks associated with GNPs, medulloblastoma, the overlap of both and peaks associated with GNPs alone or medulloblastoma alone

(Supplementary Table 1). Gene set enrichment analysis (GSEA) revealed that only genes with Gli1 promoter-binding sites associated with medulloblastoma were significantly enriched ( $P < 0.0001$ ) in JQ1-treated cells (Supplementary Fig. 5d). These results confirm the disruption of Gli1-mediated transcription by JQ1 and the preferential targeting of Gli1 transcriptional activity in tumor cells<sup>43</sup>.

#### Ectopic GLI2 expression rescues growth inhibition by JQ1

We tested whether knockdown of Brd4 could phenocopy the effects of JQ1 in Hh-driven medulloblastoma cells. As expected, knockdown of Brd4 resulted in decreased *Gli* expression (Fig. 4a,b) and cell proliferation (Fig. 4c,d), suggesting that the inhibitory effect of JQ1 was through targeting of Brd4. Furthermore, to directly assess whether BET inhibition blocked cell proliferation in Hh-driven tumor cells through targeting of *Gli* transcription, we used plasmid-based expression of GLI2 (Myc-GLI2-DN; Fig. 2f) in SmoWT-MB cells and monitored its ability to rescue the inhibition of proliferation by JQ1 (Fig. 4c). Notably, ectopic expression of GLI2 inhibited the effects of JQ1 on 5-ethynyl-2'-deoxyuridine (EdU) incorporation, resulting in levels of EdU incorporation that were nearly equivalent to levels in DMSO-treated control cells (Fig. 4e,f). This result indicates that inhibition of proliferation by JQ1 is mediated largely through inhibition of *Gli* transcription and, intriguingly, that Brd4-independent transcriptional targets of Gli transcription factors are sufficient to overcome BET inhibition.

#### SMOi-resistant Hh-driven tumors are inhibited by JQ1

Given the documented mechanisms of resistance to current, clinically available SMO inhibitors<sup>25,31</sup> and the potential of BET inhibitors as a strategy to overcome this resistance, we examined the efficacy of JQ1 in Hh-driven cancers with either acquired or *a priori* resistance to SMO inhibitors (Fig. 5a). We analyzed the efficacy of JQ1 and SMO inhibitors (GDC-0449 and LDE225) against medulloblastoma cells

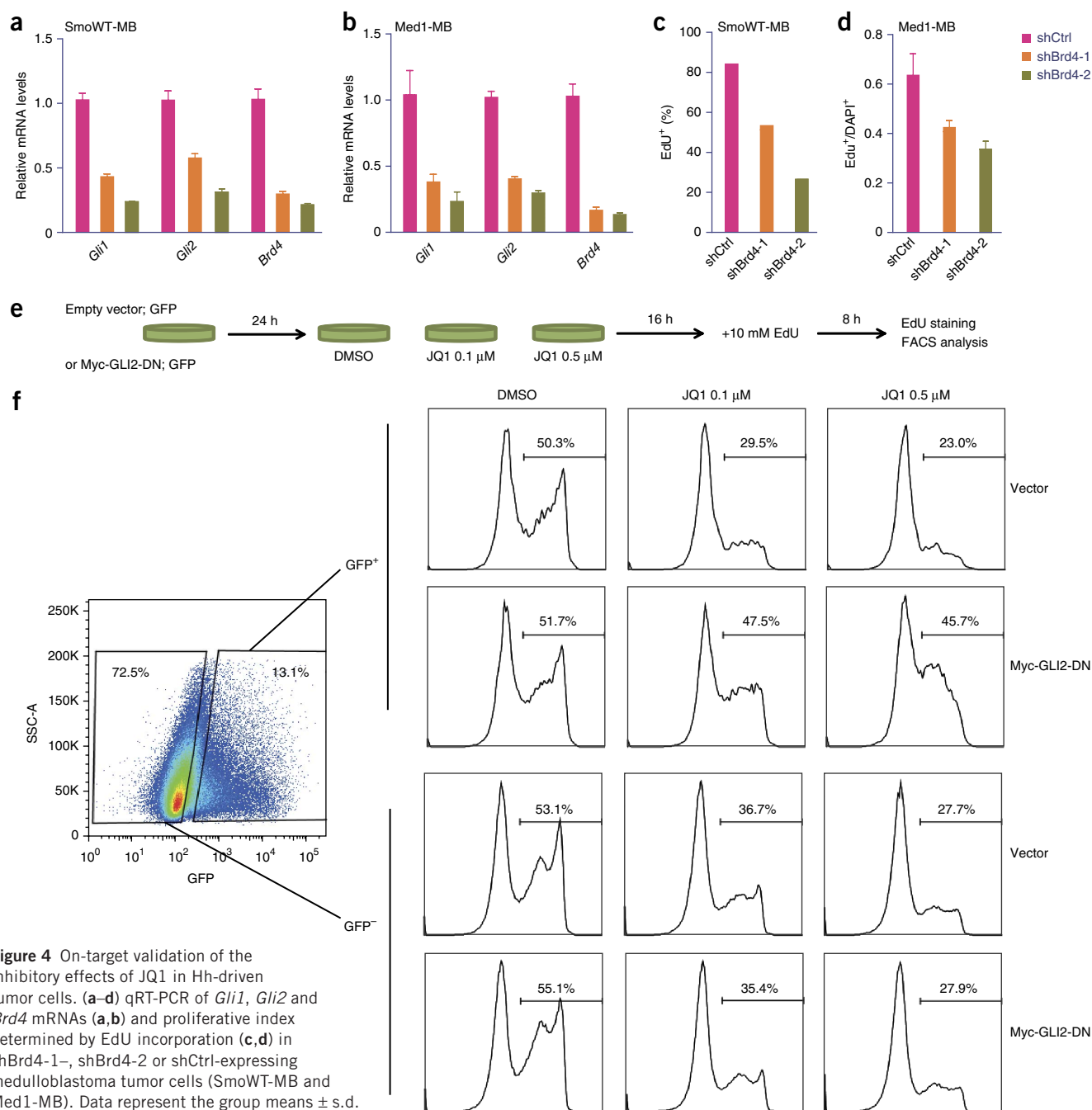


**Figure 4** On-target validation of the inhibitory effects of JQ1 in Hh-driven tumor cells. (**a–d**) qRT-PCR of *Gli1*, *Gli2* and *Brd4* mRNAs (**a,b**) and proliferative index determined by EdU incorporation (**c,d**) in shBrd4-1-, shBrd4-2 or shCtrl-expressing medulloblastoma tumor cells (SmoWT-MB and Med1-MB). Data represent the group means  $\pm$  s.d. (**e**) The schematic workflow of the GLI2-overexpressing rescue experiment in SmoWT-MB cells. (**f**) FACS analysis of EdU incorporation in SmoWT-MB cells transfected with empty vector or Myc-GLI2-DN followed by JQ1 treatment (0.1 or 0.5  $\mu$ M). GFP-expressing plasmid was used for co-transfection to mark the transfected (GFP<sup>+</sup>) cells. SSC-A, side scatter.

carrying an aspartate-to-glycine substitution at amino acid residue 477 in Smo that results in decreased sensitivity to SMO antagonists (SmoD477G-MB) (**Fig. 5b**)<sup>32</sup>; patient-derived *SUFU*-mutated primary SHH-subtype medulloblastoma cells (RCMB025); patient-derived primary atypical teratoid rhabdoid tumor (ATRT) cells (CHB\_ATRT1 and SU\_ATRT2) with derepression of *GLI1* transcription through loss of SMARCB1 (also called SNF5 or INI1) (ref. 22); and patient-derived *MYCN*-amplified primary SHH-subtype medulloblastoma cells (RCMB018). Cell viability (**Fig. 5b–f**, top), *Gli* and *GLI* levels (**Fig. 5b–f**, bottom) and EdU incorporation (**Supplementary Fig. 6a–c**) were markedly decreased in response to JQ1 in all of these

cells, and we observed little or no effect with the SMO inhibitors GDC-0449 and LDE225. Additionally, we examined *Myc*, *MYC*, *Mycn* and *MYCN* expression in SmoWT-MB, SmoD477G-MB, RCMB025, CHB\_ATRT1 and RCMB018 cells and found that *Mycn* and *MYCN* expression was consistently inhibited by JQ1 (**Fig. 5f**, bottom and **Supplementary Figs. 4h** and **6d–f**), suggesting that JQ1 targets at least two important driver oncogenes (GLI and MYCN) in these tumors.

#### **In vivo inhibition of Hh-driven tumors by JQ1**

To support a therapeutic role for BET inhibition in Hh-driven tumors, we assessed the *in vivo* efficacy of JQ1 against medulloblastomas and

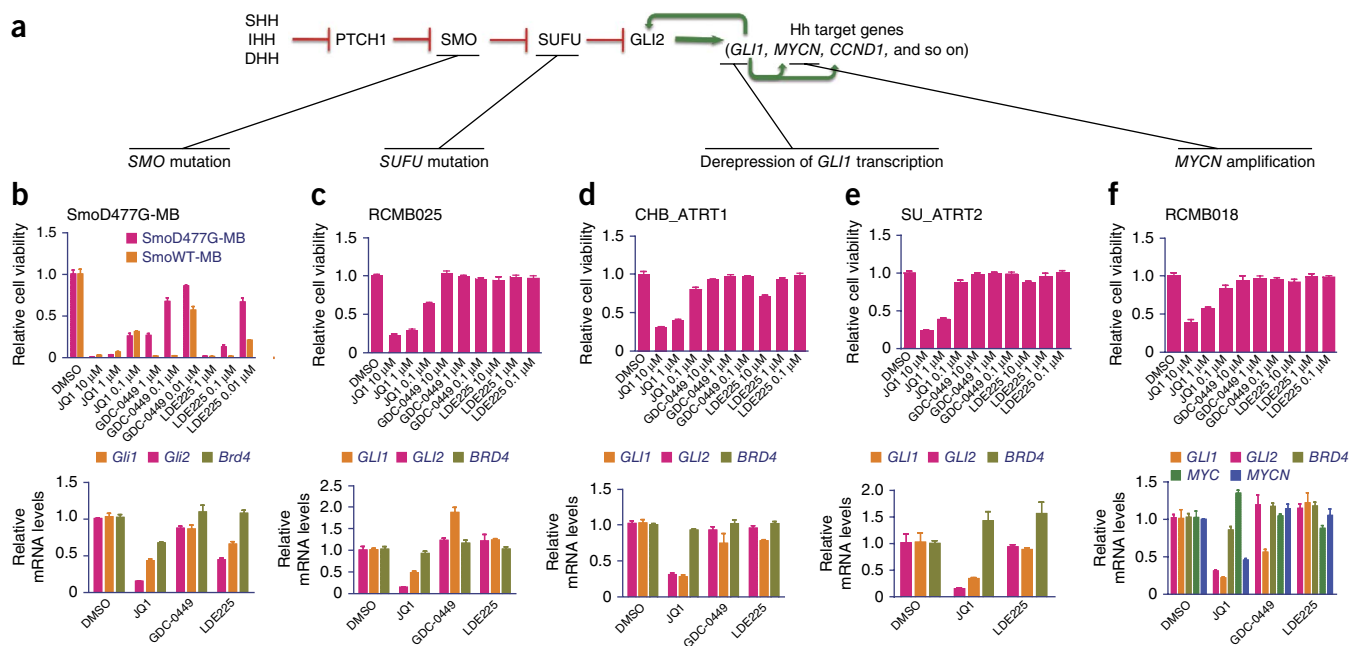


**Figure 5** JQ1 inhibits Hh pathway activity and cell viability and proliferation in SMOi-resistant Hh-driven tumors. **(a)** Schematic depicting mechanisms of resistance to Smoothened antagonists in Hh-driven cancers. **(b–f, top)** Cell viability in SMOi-resistant medulloblastoma cells (SmoD477G-MB; **b**), patient-derived *SUFU* mutant medulloblastoma cells (RCMB025; **c**), patient-derived ATRT cells (CHB\_ATRT1 and SU\_ATRT2; **d,e**) and patient-derived *MYCN*-amplified medulloblastoma cells (RCMB018; **f**) treated with increasing doses of JQ1, GDC-0449 or LDE225. Data represent the group means  $\pm$  s.d. **(b–f, bottom)** qRT-PCR of *Gli1*, *GLI1*, *Gli2*, *GLI2*, *Brd4* and *BRD4* (plus *MYC* and *MYCN* levels for RCMB018) in SmoD477G-MB (**b**), RCMB025 (**c**), CHB\_ATRT1 (**d**), SU\_ATRT2 (**e**) and RCMB018 (**f**) cells in response to JQ1 (1  $\mu$ M), GDC-0449 or LDE225 (0.1  $\mu$ M for SmoD477G-MB and 1  $\mu$ M for the other groups). Data represent the mean of triplicates  $\pm$  s.d.

BCCs. We treated flank and intracranial allografts of Med1-MB cells stably expressing a firefly luciferase reporter in immunodeficient NSG mice with either JQ1 (50 mg per kg body weight per day intraperitoneally (i.p.)) or vehicle control. We observed a significant reduction in flank tumor growth in JQ1-treated mice, as well as an increase in overall survival in JQ1-treated mice harboring intracranial allografts (**Fig. 6a,b** and **Supplementary Fig. 7a**). Additionally, we treated medulloblastoma flank allografts of SmoWT-MB or SmoD477G-MB

cells with vehicle control, JQ1 (50 mg per kg body weight per day i.p.) or GDC-0449 (100 mg per kg body weight per day orally (p.o.)). We observed marked decreases in the growth of SmoD477G-MB flank allografts in response to JQ1 but not GDC-0449, whereas SmoWT-MB flank allografts responded to both GDC-0449 and JQ1 (**Fig. 6c,d**). To evaluate the efficacy of JQ1 against BCCs *in vivo*, we used an allograft model of *Ptch*<sup>+/-</sup>; *K14-creER2*; *p53*<sup>fllox/fllox</sup>-derived mouse BCC cells<sup>34</sup>. JQ1 treatment (50 mg per kg body weight per day i.p.)

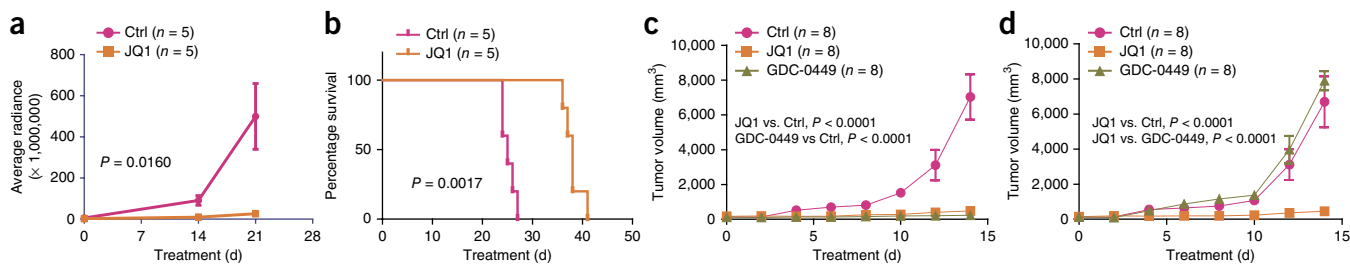


**Figure 6** JQ1 inhibits Hh-driven tumor growth *in vivo*. **(a,b)** Med1-MB cells transduced with a lentiviral luciferase reporter were used for flank (**a**) or cerebellum (**b**) injections of NSG mice, which were then randomized for treatment with either JQ1 (50 mg per kg body weight daily i.p.) or vehicle. **(a)** Tumor growth of Med1-MB allografts assessed by IVIS imaging and presented as the average radiance. **(b)** Survival curve of the mice injected with Med1-MB cells in the cerebellum. **(c,d)** Tumor growth, assessed by caliper measurement, after SmoWT-MB (**c**) and SmoD477G-MB (**d**) cells were injected into the flanks of NSG mice (both flanks of each mouse) followed by treatment with JQ1 (50 mg per kg body weight daily i.p.), GDC-0449 (100 mg per kg body weight daily p.o.) or vehicle. **(e)** Tumor growth, assessed by caliper measurement, of SMOI-naive BCC tumors generated under the dermis of NSG mice that were treated with JQ1 (50 mg per kg body weight daily i.p.), BMS-833293 (100 mg per kg body weight daily i.p.) or vehicle. Data on tumor growth represent the group means  $\pm$  s.e.m. Two-way analysis of variance (ANOVA) was used for comparing tumor growth curves. Log-rank test was used for comparing survival curves. The results shown are from two separate experiments testing JQ1 and BMS-833293, independently, but are presented on the same graph.

resulted in significant growth inhibition of BCCs but was not as effective as the clinically optimized SMO inhibitor BMS-833293 (ref. 34) (Fig. 6e). Nonetheless, in all Hh-driven tumor models tested, we observed reduction of *Gli* mRNA levels after JQ1 treatment regardless of whether allografts were sensitive or resistant to SMO inhibition (SMOi) (Supplementary Fig. 7b–f). Together these results demonstrate *in vivo* efficacy of JQ1 against Hh-driven tumors, even those with acquired or *a priori* resistance to clinically available SMO inhibitors.

## DISCUSSION

We have shown that BRD4 and other BET proteins are critical regulators of *GLI1* and *GLI2* transcription and that BET inhibition provides a new therapeutic strategy against Hh-driven tumors. Notably, as BET proteins regulate the far-downstream transcriptional output of Hh signaling, BET inhibition was effective against tumor cells that evade Smoothed antagonists through mutation of SMO or amplification of nodes downstream of SMO. Our study is clinically relevant for patients who have *a priori* resistance to SMO inhibitors and in cases in which the emergence of resistance develops after an initial response to such therapy. By acting directly on the *GLI1* and *GLI2* promoters, BET inhibition circumvents all SMOi resistance mechanisms that have been reported so far, which include mutations of SMO or *SUFU* or amplifications in *GLI2* or *MYCN*<sup>16,17,20,25,31</sup>. The response to JQ1 observed in *MYCN*-amplified SHH medulloblastoma cells (RCMB018), in terms of both decreased cell viability and *MYCN* levels, is similar to the results of a recent study showing the efficacy of BET inhibitors in *MYCN*-amplified neuroblastoma<sup>46</sup>. However, in Hh-driven tumors, it is likely that decreased *MYCN* levels in response to JQ1 treatment reflect the role of *GLI* in directly transactivating the *MYCN* promoter, in addition to the role of JQ1 in directly regulating expression of *Mycn* and *MYCN*.

Given the importance of Hh signaling in normal development, it will be essential to understand and anticipate potential toxicities of BET inhibitor therapies as they enter into clinical trials. We observed developmental anomalies at very high doses of JQ1 in our zebrafish studies (data not shown), consistent with those seen in *Brd4* heterozygous mice, which display a multitude of defects that overlap with cyclopamine-treated or Hh-deficient mice<sup>59,60</sup>. Of note, however, *Brd4* heterozygous mice develop craniofacial but not overt axial skeletal phenotypes<sup>59</sup>, unlike cyclopamine-exposed embryos<sup>2,60</sup>, suggesting lineage-specific differences of Hh pathway dependency on *Brd4*. Our finding that plasmid-driven *GLI2* expression can rescue the proliferation defect induced by JQ1 supports the existence of *GLI*-responsive promoters that do not require *BRD4* for their transactivation. Notably, such genes appear to be either individually or collectively sufficient to mediate part, if not all, of the oncogenic phenotype associated with Hh-*GLI* signaling.

Investigating how *BRD4* regulates normal Hh-mediated biological processes and documenting *BRD4*-related changes that occur during Hh-mediated oncogenic transformation could potentially elucidate factors essential for tumor development that are independent of normal development. Our analysis of gene expression changes in JQ1-treated medulloblastoma supports observations by Lee *et al.*<sup>58</sup>, who identified marked shifts in *Gli1* occupancy across the genome in medulloblastoma compared to GNPs. An unbiased characterization of *Brd4* binding across the genome in GNPs and medulloblastomas will clarify whether the genomic footprint of *Brd4* overlaps with *Gli* occupancy in the oncogenic state relative to the normal developmental state. Related to this point, emerging evidence suggests BET proteins

converge on super-enhancer sites across the genome and that these super-enhancer sites help transactivate promoters of key regulators of cellular identity in normal and pathogenic contexts<sup>42,43</sup>. Whether *GLI* transactivates super enhancer-related promoters and, accordingly, whether super-enhancer sites are positioned over *GLI* promoters is currently under active investigation.

## METHODS

Methods and any associated references are available in the online version of the paper.

**Accession codes.** Gene expression profiling data has been deposited into the National Center for Biotechnology Information (NCBI) Gene Expression Omnibus (GEO) with accession code [GSE58185](https://www.ncbi.nlm.nih.gov/geo/query/acc.cgi?acc=GSE58185).

*Note: Any Supplementary Information and Source Data files are available in the online version of the paper.*

## ACKNOWLEDGMENTS

This work was supported the St. Baldrick's Foundation Scholar Award (Y.-J.C.), a Beirne Faculty Scholar Endowment (Y.-J.C.), US National Institutes of Health (NIH) grant U01-CA176287 (Y.-J.C.), an Alex's Lemonade Stand Foundation Young Investigator Award (Y.T.), the Damon-Runyon Cancer Research Foundation (J.Q. and J.E.B.), NIH R01-CA159859 (R.W.-R.) and a pilot project grant from the Medical College of Wisconsin Cancer Center—Advancing a Healthier Wisconsin (B.A.L.). R.W.-R. is the recipient of a Leadership Award (LA1-01747) from the California Institute of Regenerative Medicine. We thank the Stanford Functional Genomics Facility (SFGF) and the Protein and Nucleic Acid (PAN) facility for their assistance in generating gene expression microarray data and reagents. We thank M. Scott (Stanford), C. Rudin (Memorial Sloan-Kettering Cancer Center), P. Beachy (Stanford), A. Sweet-Cordero (Stanford), P.-T. Chang (University of California, San Francisco), R. Karlstrom (University of Massachusetts, Amherst) and J.K. Chen (Stanford) for reagents, helpful suggestions and/or critical reading of the manuscript.

## AUTHOR CONTRIBUTIONS

Y.T. and Y.-J.C. conceived the project and wrote the manuscript. Y.T., B.N., S.M., B.B., N.V., S.S., S.C., A.P., S.O. and F.Y. performed all molecular biology experiments. J.Q. and J.E.B. synthesized and supplied JQ1 for all studies. A.E.O., S.X.A., R.J.W., A.L. and J.Y.T. generated and prepared GEMM-derived BCC cells, and R.W.-R. generated and provided patient-derived medulloblastoma cells. P.B., G.B., R.B. and Y.-J.C. performed all informatics analyses. S.G., A.L., Y.T., S.M., P.W., M.M., S.H.C. and S.S. performed JQ1 mouse *in vivo* studies. M.I.W. and B.A.L. performed all zebrafish studies.

## COMPETING FINANCIAL INTERESTS

The authors declare competing financial interests: details are available in the online version of the paper.

Reprints and permissions information is available online at <http://www.nature.com/reprints/index.html>.

- Goodrich, L.V., Johnson, R.L., Milenkovic, L., McMahon, J.A. & Scott, M.P. Conservation of the hedgehog/patched signaling pathway from flies to mice: induction of a mouse patched gene by Hedgehog. *Genes Dev.* **10**, 301–312 (1996).
- Binns, W., Shupe, J.L., Keeler, R.F. & James, L.F. Chronologic evaluation of teratogenicity in sheep fed *Veratrum californicum*. *J. Am. Vet. Med. Assoc.* **147**, 839–842 (1965).
- Gorlin, R.J., Vickers, R.A., Kellen, E. & Williamson, J.J. Multiple nasal-cell nevi syndrome. An analysis of a syndrome consisting of multiple nevoid basal-cell carcinoma, jaw cysts, skeletal anomalies, medulloblastoma, and hyporesponsiveness to parathormone. *Cancer* **18**, 89–104 (1965).
- Johnson, R.L. *et al.* Human homolog of patched, a candidate gene for the basal cell nevus syndrome. *Science* **272**, 1668–1671 (1996).
- Echelard, Y. *et al.* Sonic hedgehog, a member of a family of putative signaling molecules, is implicated in the regulation of CNS polarity. *Cell* **75**, 1417–1430 (1993).
- Marigo, V. *et al.* Cloning, expression, and chromosomal location of SHH and IHH: two human homologues of the *Drosophila* segment polarity gene hedgehog. *Genomics* **28**, 44–51 (1995).
- Alcedo, J., Ayzenzon, M., Von Ohlen, T., Noll, M. & Hooper, J.E. The *Drosophila* smoothed gene encodes a seven-pass membrane protein, a putative receptor for the hedgehog signal. *Cell* **86**, 221–232 (1996).

8. Huangfu, D. & Anderson, K.V. Cilia and Hedgehog responsiveness in the mouse. *Proc. Natl. Acad. Sci. USA* **102**, 11325–11330 (2005).
9. Haycraft, C.J. *et al.* Gli2 and Gli3 localize to cilia and require the intraflagellar transport protein polaris for processing and function. *PLoS Genet.* **1**, e53 (2005).
10. Liu, A., Wang, B. & Niswander, L.A. Mouse intraflagellar transport proteins regulate both the activator and repressor functions of Gli transcription factors. *Development* **132**, 3103–3111 (2005).
11. Oliver, T.G. *et al.* Transcriptional profiling of the Sonic hedgehog response: a critical role for N-myc in proliferation of neuronal precursors. *Proc. Natl. Acad. Sci. USA* **100**, 7331–7336 (2003).
12. Regl, G. *et al.* Human GLI2 and GLI1 are part of a positive feedback mechanism in basal cell carcinoma. *Oncogene* **21**, 5529–5539 (2002).
13. Mao, J. *et al.* A novel somatic mouse model to survey tumorigenic potential applied to the Hedgehog pathway. *Cancer Res.* **66**, 10171–10178 (2006).
14. Xie, J. *et al.* Mutations of the PATCHED gene in several types of sporadic extracutaneous tumors. *Cancer Res.* **57**, 2369–2372 (1997).
15. Thayer, S.P. *et al.* Hedgehog is an early and late mediator of pancreatic cancer tumorigenesis. *Nature* **425**, 851–856 (2003).
16. Cho, Y.J. *et al.* Integrative genomic analysis of medulloblastoma identifies a molecular subgroup that drives poor clinical outcome. *J. Clin. Oncol.* **29**, 1424–1430 (2011).
17. Pugh, T.J. *et al.* Medulloblastoma exome sequencing uncovers subtype-specific somatic mutations. *Nature* **488**, 106–110 (2012).
18. Taylor, M.D. *et al.* Mutations in SUFU predispose to medulloblastoma. *Nat. Genet.* **31**, 306–310 (2002).
19. ten Haaf, A. *et al.* Expression of the glioma-associated oncogene homolog (GLI) 1 in human breast cancer is associated with unfavourable overall survival. *BMC Cancer* **9**, 298 (2009).
20. Northcott, P.A. *et al.* Subgroup-specific structural variation across 1,000 medulloblastoma genomes. *Nature* **488**, 49–56 (2012).
21. Buczkowicz, P., Ma, J. & Hawkins, C. GLI2 is a potential therapeutic target in pediatric medulloblastoma. *J. Neuropathol. Exp. Neurol.* **70**, 430–437 (2011).
22. Jagani, Z. *et al.* Loss of the tumor suppressor Snf5 leads to aberrant activation of the Hedgehog-Gli pathway. *Nat. Med.* **16**, 1429–1433 (2010).
23. Zwerner, J.P. *et al.* The EWS/FLI1 oncogenic transcription factor deregulates GLI1. *Oncogene* **27**, 3282–3291 (2008).
24. Chen, J.K., Taipale, J., Cooper, M.K. & Beachy, P.A. Inhibition of Hedgehog signaling by direct binding of cyclopamine to Smoothened. *Genes Dev.* **16**, 2743–2748 (2002).
25. Buonamici, S. *et al.* Interfering with resistance to smoothened antagonists by inhibition of the PI3K pathway in medulloblastoma. *Sci. Transl. Med.* **2**, 51ra70 (2010).
26. Lee, M.J. *et al.* Hedgehog pathway inhibitor saridegib (IPI-926) increases lifespan in a mouse medulloblastoma model. *Proc. Natl. Acad. Sci. USA* **109**, 7859–7864 (2012).
27. Zhang, Y., Latterra, J. & Pomper, M.G. Hedgehog pathway inhibitor HhAntag691 is a potent inhibitor of ABCG2/BCRP and ABCB1/Pgp. *Neoplasia* **11**, 96–101 (2009).
28. LoRusso, P.M. *et al.* Phase I trial of hedgehog pathway inhibitor vismodegib (GDC-0449) in patients with refractory, locally advanced or metastatic solid tumors. *Clin. Cancer Res.* **17**, 2502–2511 (2011).
29. Rudin, C.M. *et al.* Treatment of medulloblastoma with hedgehog pathway inhibitor GDC-0449. *N. Engl. J. Med.* **361**, 1173–1178 (2009).
30. Von Hoff, D.D. *et al.* Inhibition of the hedgehog pathway in advanced basal-cell carcinoma. *N. Engl. J. Med.* **361**, 1164–1172 (2009).
31. Yauch, R.L. *et al.* Smoothened mutation confers resistance to a Hedgehog pathway inhibitor in medulloblastoma. *Science* **326**, 572–574 (2009).
32. Kim, J. *et al.* Itraconazole and arsenic trioxide inhibit Hedgehog pathway activation and tumor growth associated with acquired resistance to smoothened antagonists. *Cancer Cell* **23**, 23–34 (2013).
33. Kim, J., Lee, J.J., Gardner, D. & Beachy, P.A. Arsenic antagonizes the Hedgehog pathway by preventing ciliary accumulation and reducing stability of the Gli2 transcriptional effector. *Proc. Natl. Acad. Sci. USA* **107**, 13432–13437 (2010).
34. Atwood, S.X., Li, M., Lee, A., Tang, J.Y. & Oro, A.E. GLI activation by atypical protein kinase C  $\nu\lambda$  regulates the growth of basal cell carcinomas. *Nature* **494**, 484–488 (2013).
35. Kenney, A.M., Widlund, H.R. & Rowitch, D.H. Hedgehog and PI-3 kinase signaling converge on Nmyc1 to promote cell cycle progression in cerebellar neuronal precursors. *Development* **131**, 217–228 (2004).
36. Hyman, J.M. *et al.* Small-molecule inhibitors reveal multiple strategies for Hedgehog pathway blockade. *Proc. Natl. Acad. Sci. USA* **106**, 14132–14137 (2009).
37. Filippakopoulos, P. *et al.* Selective inhibition of BET bromodomains. *Nature* **468**, 1067–1073 (2010).
38. Dhalluin, C. *et al.* Structure and ligand of a histone acetyltransferase bromodomain. *Nature* **399**, 491–496 (1999).
39. Jacobson, R.H., Ladurner, A.G., King, D.S. & Tjian, R. Structure and function of a human TAFII250 double bromodomain module. *Science* **288**, 1422–1425 (2000).
40. Jang, M.K. *et al.* The bromodomain protein Brd4 is a positive regulatory component of P-TEFb and stimulates RNA polymerase II-dependent transcription. *Mol. Cell* **19**, 523–534 (2005).
41. Yang, Z. *et al.* Recruitment of P-TEFb for stimulation of transcriptional elongation by the bromodomain protein Brd4. *Mol. Cell* **19**, 535–545 (2005).
42. Whyte, W.A. *et al.* Master transcription factors and mediator establish super-enhancers at key cell identity genes. *Cell* **153**, 307–319 (2013).
43. Lovén, J. *et al.* Selective inhibition of tumor oncogenes by disruption of super-enhancers. *Cell* **153**, 320–334 (2013).
44. Delmore, J.E. *et al.* BET bromodomain inhibition as a therapeutic strategy to target c-Myc. *Cell* **146**, 904–917 (2011).
45. Mertz, J.A. *et al.* Targeting MYC dependence in cancer by inhibiting BET bromodomains. *Proc. Natl. Acad. Sci. USA* **108**, 16669–16674 (2011).
46. Puissant, A. *et al.* Targeting MYCN in neuroblastoma by BET bromodomain inhibition. *Cancer Discov.* **3**, 308–323 (2013).
47. Bandopadhyay, P. *et al.* BET bromodomain inhibition of MYC-amplified medulloblastoma. *Clin. Cancer Res.* **20**, 912–925 (2014).
48. Chen, J.K., Taipale, J., Young, K.E., Maiti, T. & Beachy, P.A. Small molecule modulation of Smoothened activity. *Proc. Natl. Acad. Sci. USA* **99**, 14071–14076 (2002).
49. Maity, T., Fuse, N. & Beachy, P.A. Molecular mechanisms of Sonic hedgehog mutant effects in holoprosencephaly. *Proc. Natl. Acad. Sci. USA* **102**, 17026–17031 (2005).
50. Lewis, K.E., Concordet, J.P. & Ingham, P.W. Characterisation of a second patched gene in the zebrafish *Danio rerio* and the differential response of patched genes to Hedgehog signalling. *Dev. Biol.* **208**, 14–29 (1999).
51. Shen, M.C. *et al.* Heat-shock-mediated conditional regulation of hedgehog/gli signaling in zebrafish. *Dev. Dyn.* **242**, 539–549 (2013).
52. Macdonald, R. *et al.* Midline signalling is required for Pax gene regulation and patterning of the eyes. *Development* **121**, 3267–3278 (1995).
53. Lee, J. *et al.* An ENU mutagenesis screen in zebrafish for visual system mutants identifies a novel splice-acceptor site mutation in patched2 that results in colobomas. *Invest. Ophthalmol. Vis. Sci.* **53**, 8214–8221 (2012).
54. Chen, M.H. *et al.* Cilium-independent regulation of Gli protein function by Sufu in Hedgehog signaling is evolutionarily conserved. *Genes Dev.* **23**, 1910–1928 (2009).
55. Roessler, E. *et al.* A previously unidentified amino-terminal domain regulates transcriptional activity of wild-type and disease-associated human GLI2. *Hum. Mol. Genet.* **14**, 2181–2188 (2005).
56. Goodrich, L.V., Milenkovic, L., Higgins, K.M. & Scott, M.P. Altered neural cell fates and medulloblastoma in mouse patched mutants. *Science* **277**, 1109–1113 (1997).
57. Aszterbaum, M. *et al.* Ultraviolet and ionizing radiation enhance the growth of BCCs and trichoblastomas in patched heterozygous knockout mice. *Nat. Med.* **5**, 1285–1291 (1999).
58. Lee, E.Y. *et al.* Hedgehog pathway-regulated gene networks in cerebellum development and tumorigenesis. *Proc. Natl. Acad. Sci. USA* **107**, 9736–9741 (2010).
59. Houzelstein, D. *et al.* Growth and early postimplantation defects in mice deficient for the bromodomain-containing protein Brd4. *Mol. Cell. Biol.* **22**, 3794–3802 (2002).
60. Cooper, M.K., Porter, J.A., Young, K.E. & Beachy, P.A. Teratogen-mediated inhibition of target tissue response to Shh signaling. *Science* **280**, 1603–1607 (1998).

## ONLINE METHODS

**Ethics statement.** All studies were performed under approval and oversight by the Institutional Review Board committees of Stanford University, Boston Children's Hospital and Rady Children's Hospital/Sanford-Burnham Medical Research Institute.

**Cell lines and drug reagents.** Mouse BCC (ASZ001), 293T and Hh-Light2 cells were derived and maintained as previously described<sup>24,34,57</sup>. RCMB025 and RCMB018 cells were derived from primary surgical resections of two medulloblastoma cases at Rady Children's Hospital and were further characterized by whole-genome sequencing as having a *SUFU* mutation and *MYCN* amplification, respectively<sup>61</sup>. CHB\_ATRT1 cells were derived from tumor obtained at the time of primary surgical resection of a posterior fossa ATRT at Boston Children's Hospital. SU\_ATRT2 cells were derived from tumor obtained at the time of surgical resection of an intraventricular ATRT at Lucile Packard Children's Hospital/Stanford University Medical Center. Med1-MB cells, generated from a spontaneous tumor arising in a *Ptch*<sup>+/-</sup>; *lacZ* mouse, were kindly provided by M. Scott (Stanford). SmoWT-MB and SmoD477G-MB cells isolated from either parental SmoWT or SmoD477G mouse *Ptch*<sup>+/-</sup>; *p53*<sup>-/-</sup> MB hind-flank allografts were kindly provided by C. Rudin (Memorial Sloan-Kettering Cancer Center). *Sufu*<sup>-/-</sup> MEFs (conditional deletion of exons 4–8 (ref. 54)) were kindly provided by P.-T. Chang (University of California, San Francisco). SAG, SANT-1, GDC-0449 (S1082, Vismodegib, HhAntag691) and LDE225 (S2151, NVP-LDE225, Erismodegib) were purchased from SelleckChem.com. Shh-N CM was kindly provided by P. Beachy (Stanford). JQ1 was synthesized as previously described<sup>44</sup>.

**RNA extraction and qRT-PCR.** RNA was extracted using QIAzol Lysis Reagent (79306, Qiagen, Venlo, Netherland) per the manufacturer's instructions. Reverse transcription was performed with 1 µg total RNA using the High Capacity cDNA Reverse Transcription Kit (4368813, Invitrogen). Real-time qPCR was performed using 2× Maxima SYBR Green qPCR Master Mix (#K0251, Thermo Scientific) on an Eppendorf Mastercycler PCR machine. The qPCR primers used are listed in **Supplementary Table 2**.

**Cell cycle, proliferation, viability and apoptosis assays.** For cell cycle analysis, cells were fixed in 70% ethanol for 30 min at 4 °C. After two washes with cold PBS, fixed cells were resuspended in staining buffer (200 µl PBS + 10 µl 1 mg ml<sup>-1</sup> propidium iodide + 2 µl 100 mg ml<sup>-1</sup> RNase A) and incubated at 37 °C for 45 min. Cells were washed once with cold PBS and filtered through a 70-µm mesh (ELKO Filtering Co., Miami, FL, USA). Filtered cells were centrifuged and resuspended in 500 µl PBS for FACS analysis. Proliferation assays were performed by culturing cells in the presence of 10 µM EdU for 6–8 h. The EdU<sup>+</sup> population was determined using either the Click-iT EdU Alexa Fluor 488 Flow Cytometry Assay Kit (C35002, Invitrogen, CA, USA) or the Click-iT EdU Alexa Fluor 594 Imaging Kit (C10339, Invitrogen, CA, USA). Cells were counterstained with DAPI (D8417, Sigma, MO, USA), and the proliferation index was calculated as EdU<sup>+</sup>/DAPI<sup>+</sup> cells. Apoptosis was analyzed using the BD Pharmingen FITC Annexin V Apoptosis Detection kit I (Cat# 556547, BD Biosciences, CA, USA) per the manufacturer's instructions. Cell viability was assessed using CellTiter-Glo (G7573, Promega, WI, USA) according to the manufacturer's instructions. Cells were plated at 5,000 cells per well in 96-well plates and treated with drugs as indicated, and data were collected on a TECAN Infinite 200 plate reader. The drug synergy between JQ1 and GDC-0449 was calculated using CalcuSyn software (Biosoft, Cambridge, UK). A combination index less than 1 was considered as synergistic. All FACS data were collected on a BD Fortessa analyzer (BD Biosciences, CA, USA), and data analyses were performed using Flowjo software (Tree Star, OR, USA).

**GLI2 overexpression.** The Myc-GLI2-DN (17649, pCS2-MT-GLI2-ΔN) plasmid was purchased from Addgene (Cambridge, MA, USA). The 3×HA-Gli2-FL plasmid was kindly provided by P. Beachy (Stanford). Plasmid transfection was performed using Turbofect transfection reagent (#R0531, Thermo Scientific) according to the manufacturer's instructions. Cells were treated with drugs 24 h after transfection as indicated.

**Western blot analysis.** Cells were lysed with RIPA buffer (sc-24948, Santa Cruz Biotechnology) for 30 min on ice, and lysates were cleared by centrifugation at 13,000 r.p.m. for 15 min at 4 °C. Supernatants were incubated with 4× Laemmli sample buffer (#161-0747, Bio-rad) at 95 °C for 5 min. The samples were then separated with SDS-PAGE gel and immunoblotted with the indicated antibodies: anti-HA (ab18181, Abcam; 1:5,000 dilution), anti-c-Myc (sc-789, Santa Cruz Biotechnology; 1:1,000 dilution), anti-GLI1 (#2643, Cell signaling; 1:1,000 dilution) and anti-β-tubulin (ab6046, Abcam; 1:5,000 dilution).

**Lentiviral infection.** shRNA lentiviral constructs against mouse *Brd2*, *Brd3* and *Brd4* (The RNAi Consortium mouse collection) were kindly provided by A. Sweet-Cordero (Stanford), and shRNA insertion sequences were confirmed by Sanger sequencing. To produce shRNA lentiviruses, 293T cells were transfected with a lentiviral vector and packaging plasmids (pDelta 8.92 + VSV-G). Titters were collected 48 h after transfection and concentrated by polyethylene glycol precipitation. The precipitated lentivirus was resuspended in PBS and aliquoted for storage at –80 °C. For shRNA lentivirus infection, cells were incubated with shRNA lentivirus for 16 h. At 48 h after infection, puromycin was added to select virally infected cells for further experiments.

**Dual-luciferase reporter assay.** Hh-Light2 cells were cultured until confluent and treated with drugs as indicated. Dual-luciferase reporter assays were performed using the Dual-Luciferase Reporter Assay System 10-Pack (E1960, Promega, WI, USA) according to manufacturer's instructions, and data were collected on a TECAN Infinite 200 plate reader.

**ChIP-qPCR.** Cells were fixed with 1% formaldehyde for 10 min at room temperature before adding glycine to stop the fixation. The cells were then harvested, snap frozen and stored at –80 °C before use. For each ChIP experiment, chromatin isolated from 10<sup>6</sup> to 10<sup>7</sup> cells was sonicated and immunoprecipitated with 3–5 µg of the indicated antibody and 100 µl Dynabeads protein G. Beads were washed five times with RIPA buffer and one time with Tris + EDTA containing 50 mM NaCl. Bound complexes were eluted by heating at 65 °C with occasional vortexing for 30 min, and crosslinking was reversed by overnight incubation at 65 °C. INPUT DNA was also treated for crosslink reversal. Immunoprecipitated DNA and INPUT DNA were then purified by RNaseA/proteinase K treatment, phenol:chloroform extraction and ethanol precipitation. qPCR was performed using 2× Maxima SYBR Green qPCR Master Mix (#K0251, Thermo Scientific) on an Eppendorf Mastercycler PCR machine. The ChIP-qPCR primer sequences used are listed in **Supplementary Table 2**.

**Gene expression microarray analysis.** All gene expression profiling data has been deposited into the National Center for Biotechnology Information (NCBI) Gene Expression Omnibus (GEO) with accession code [GSE58185](https://www.ncbi.nlm.nih.gov/geo/query/acc.cgi?acc=GSE58185).

Gene expression data were generated from total RNA derived from biological duplicates of SmoWT-MB cells treated with control (DMSO), JQ1 (1 µM) or GDC-0449 (0.1 µM) for 6 h. RNA was hybridized to Illumina MouseWG-6 v2.0 (SmoWT-MB) expression bead arrays per the manufacturer's instructions. Rank-invariant normalized data were generated using GenomeStudio v1.9.0 and converted to .gct file format, which was then collapsed to gene symbols using the GSEA desktop application (<http://www.broadinstitute.org/gsea/index.jsp>). Differentially expressed genes were visualized using the GENE-E desktop application (<http://www.broadinstitute.org/cancer/software/GENE-E/>), and the top 5,000 differentially expressed genes between drug-treated and control-treated cells were used for agglomerative hierarchical clustering using Pearson correlation and the average linkage metric across samples and genes.

Comparative marker selection analysis between JQ1- or GDC-0449- and DMSO-treated cells was performed in GenePattern using the default settings. Genes with a *P* value less than 0.05 and a *q* value less than 0.1 were considered to be significantly differentially expressed. We performed  $\chi^2$  analysis to determine the significance of the overlap between genes that were downregulated by JQ1 and GDC-0449. To identify gene sets differentially expressed after treatment with JQ1 or GDC-0449 (compared to DMSO-treated controls), GSEA was performed as previously described<sup>62</sup> using the C2cpq gene set (MSigDB). Gene sets with a nominal *P* value less than 0.05 and *q* value less than 0.25 were considered

significant. We performed Fisher's exact test to determine the significance of the overlap between gene sets that were downregulated by JQ1 and GDC-0449.

GSEA was also performed using gene sets (.gmt files) derived from Puissant *et al.*<sup>46</sup>, Atwood *et al.*<sup>34</sup> and Lee *et al.*<sup>58</sup> (**Supplementary Table 1**). Briefly, genes associated with Gli1 ChIP-chip peaks in normal GNPs and medulloblastoma (listed in **Supplementary Table 1a,b** from Lee *et al.*<sup>58</sup>) were converted to gene sets (Lee\_Gli1\_GNP and Lee\_Gli1\_MB). We then used the Venn diagram function in GENE-E to generate gene sets of overlapping and distinct genes between these lists (Lee\_Gli1\_GNP\_only, Lee\_Gli1\_MB\_only and Lee\_Gli1\_GNP\_MB\_overlap).

**In vivo mouse studies.** *In vivo* efficacy studies were performed in accordance with protocols approved by the Institutional Animal Care and Use Committee at Stanford University and Children's Hospital Research Center Oakland. SMOi-naive BCC allografts were derived from BCC tumors generated in *Ptch*<sup>+/-</sup>; *K14-creER2*; *p53*<sup>flox/flox</sup> mice as previously described<sup>34</sup>. Tumors were treated with vehicle control, BMS-833293 (Bristol Myers Squibb Hedgehog inhibitor) (100 mg per kg daily i.p.) or JQ1 (50 mg per kg daily i.p.) until euthanasia was required when the size of vehicle-treated tumors exceeded the limit in our animal care guidelines. Tumor size was measured with calipers every 3–4 d. Tumors were also harvested for RNA analysis. SMOi-resistant mouse BCCs were generated by treating SMOi-naive BCC allografts with BMS-833293 in a cyclical fashion and then with JQ1 as described above. The tumors were treated with JQ1 (50 mg per kg daily i.p.) or vehicle for 7 d before harvesting for RNA analysis.

For *in vivo* medulloblastoma studies, SmoWT-MB, SmoD477G-MB and GFP-luciferase-transduced Med1-MB cells were used for flank or cerebellum injections.  $2 \times 10^6$  cells were injected into the flank of each 4- to 6-week-old *NOD.Cg-Prkdcscid Il2rgtm1 Wjl/SzJ* (NSG) mouse (The Jackson Laboratories).  $0.5 \times 10^6$  cells were used for cerebellum injection, as previously described<sup>32</sup>. After engraftments were confirmed, mice were randomized into treatment and control groups and treated with vehicle control, GDC-0449 (100 mg per kg body weight daily p.o.) or JQ1 (50 mg per kg body weight daily i.p.) until euthanasia was required. Tumor growth was measured with calipers or monitored by IVIS imaging on a Xenogen IVIS2000 (Perkin-Elmer). At the end of

treatment, tumors were harvested in RNAlater for RNA analysis. Survival data were recorded for the cerebellum-injected mice using Med1-MB cells.

**Zebrafish studies.** All fish studies were performed in accordance with protocols approved by the Institutional Animal Care and Use Committee at the Medical College of Wisconsin. Zebrafish embryos from an outcross of Tg(*GBS-ptch2:eGFP*)<sup>+/-</sup> with TL (Tübingen long-fin) WT were exposed to JQ1 at concentrations ranging from 0.25 to 5  $\mu$ M. A 0.6  $\mu$ M working dose was determined to be optimal for *in vivo* studies, as it caused no phenotype, in contrast to 0.75  $\mu$ M, which caused elevated cell death and dysmorphology. The *ptch2*:GFP reporter fish were then exposed to JQ1, cyclopamine (25  $\mu$ M) or vehicle control (DMSO or EtOH for JQ1 and cyclopamine, respectively) from 2 to 30 hpf and then fixed with 4% paraformaldehyde for *in situ* hybridization using a GFP probe and fast red. All fish with GFP positivity were scored for intensity of staining.

For Shh overexpression experiments, embryos from a Tg(*hsp70l:Shha-eGFP*)<sup>+/-</sup>  $\times$  TL WT cross were collected and heat shocked at 38 °C for 15 min at the eight-somite stage. After heat shock, the embryos were immediately placed in JQ1 at a 0.6  $\mu$ M or 6.0  $\mu$ M concentration. DMSO was used as a negative control. At 12 hpf, GFP-positive and GFP-negative embryos were sorted, and embryos were transferred to equivalent concentrations of fresh drug or DMSO. Images were captured using a Nikon Coolpix digital P520 camera fitted to a Lieca MZLIII stereo microscope at 30 and 56 hpf. Embryos were scored for eye size (dorsal axis length) at 56 hpf.

**Statistical analyses.** Two-way ANOVA was used for comparing tumor growth curves. Log-rank test was used for comparing survival curves.  $\chi^2$  or Fisher's exact test was used for statistical analyses of contingency table data. Student's *t* test was used for all the other comparisons.

61. Kool, M. *et al.* Genome sequencing of SHH medulloblastoma predicts genotype-related response to Smoothened inhibition. *Cancer Cell* **25**, 393–405 (2014).
62. Subramanian, A. *et al.* Gene set enrichment analysis: a knowledge-based approach for interpreting genome-wide expression profiles. *Proc. Natl. Acad. Sci. USA* **102**, 15545–15550 (2005).